AMERICAN SOCIETY FOR MICROBIOLOGY | Journal of Virology

Nipah Virus Matrix Protein Influences Fusogenicity and Is Essential for Particle Infectivity and Stability

Erik Dietzel,[a] Larissa Kolesnikova,[a] Bevan Sawatsky,[b,c] Anja Heiner,[a] Michael Weis,[a] Gary P. Kobinger,[d,e,f] Stephan Becker,[a,g] Veronika von Messling,[b,c,g] Andrea Maisner[a]

Institute of Virology, Philipps University Marburg, Marburg, Germany[a]; INRS-Institut Armand-Frappier, University of Quebec, Laval, Quebec, Canada[b]; Veterinary Medicine Division, Paul-Ehrlich-Institut, Langen, Germany[c]; National Microbiology Laboratory, Public Health Agency of Canada, Winnipeg, Manitoba, Canada[d]; Department of Medical Microbiology, University of Manitoba, Winnipeg, Manitoba, Canada[e]; Department of Immunology, University of Manitoba, Winnipeg, Manitoba, Canada[f]; German Center for Infection Research, Partner Site Giessen-Marburg-Langen, Germany[g]

ABSTRACT

Nipah virus (NiV) causes fatal encephalitic infections in humans. To characterize the role of the matrix (M) protein in the viral life cycle, we generated a reverse genetics system based on NiV strain Malaysia. Using an enhanced green fluorescent protein (eGFP)-expressing M protein-deleted NiV, we observed a slightly increased cell-cell fusion, slow replication kinetics, and significantly reduced peak titers compared to the parental virus. While increased amounts of viral proteins were found in the supernatant of cells infected with M-deleted NiV, the infectivity-to-particle ratio was more than 100-fold reduced, and the particles were less thermostable and of more irregular morphology. Taken together, our data demonstrate that the M protein is not absolutely required for the production of cell-free NiV but is necessary for proper assembly and release of stable infectious NiV particles.

IMPORTANCE

Henipaviruses cause a severe disease with high mortality in human patients. Therefore, these viruses can be studied only in biosafety level 4 (BSL-4) laboratories, making it more challenging to characterize their life cycle. Here we investigated the role of the Nipah virus matrix protein in virus-mediated cell-cell fusion and in the formation and release of newly produced particles. We found that even though low levels of infectious viruses are produced in the absence of the matrix protein, it is required for the release of highly infectious and stable particles. Fusogenicity of matrixless viruses was slightly enhanced, further demonstrating the critical role of this protein in different steps of Nipah virus spread.

Nipah virus (NiV) is a zoonotic paramyxovirus in the *Henipavirus* genus that originates from *Pteropus* bats. It causes sporadic outbreaks of deadly encephalitic disease in humans in Malaysia, Singapore, India, and Bangladesh (1, 2). Cross-reactive antibodies against NiV and other related henipaviruses have been detected in bats and pigs as far afield as Africa and other parts of Southeast Asia, indicating that these viruses circulate quite widely (3–10).

NiV entry and cell-to-cell spread are driven by two transmembrane glycoproteins, the attachment (G) and the fusion (F) proteins, that are exposed on the surface of viral particles and on infected cells to mediate attachment to the host cell receptor and membrane fusion, respectively. The viral matrix (M) protein associates with the inner leaflet of the plasma membrane mediating the contact between the ribonucleoprotein (RNP) complex and the surface glycoproteins. Though the detailed role varies between different viruses, paramyxoviral M proteins are generally considered the main drivers of assembly (11). Supporting the idea of a critical role in virus particle formation and budding, NiV M protein forms virus-like particles (VLPs) when expressed on its own (12, 13), and it drives apical assembly and budding of NiV virions in polarized epithelial cells (14). Trafficking of NiV M is a complex process involving transit through the nucleus (15–18), despite replication occurring exclusively in the cytoplasm. When NiV M protein nuclear localization or export signals are interrupted, or if the endosomal sorting complexes required for transport (ESCRT) pathway-interacting late domains are disrupted, NiV M proteins lose their ability to accumulate at the plasma membrane and no longer generate virus-like particles (12, 17, 19). Aside from the M protein, the NiV glycoproteins appear to also possess intrinsic budding capabilities (13), but their roles in viral egress remain unresolved.

So far, only two paramyxoviruses, measles virus (MV) and human respiratory syncytial virus (HRSV), have been successfully rescued without transcomplementation by plasmid-encoded M protein (20, 21). We show here that a recombinant enhanced green fluorescent protein (eGFP)-expressing M protein-deficient NiV (NiVeGΔM) could be recovered and propagated in the absence of any exogenous M expression. NiVeGΔM was detected in the culture supernatant, though virus titers were up to 1,000-fold lower than for the parental wild-type (wt) virus, and cell-free viruses were less stable at 37°C. NiVeGΔM also displayed enhanced fusion kinetics, suggesting that the M protein plays a role in downregulation of the F/G-mediated cell-cell fusion. Taken together, our data show that the M protein plays an important role for the

Received 17 November 2015 **Accepted** 10 December 2015

Accepted manuscript posted online 16 December 2015

Citation Dietzel E, Kolesnikova L, Sawatsky B, Heiner A, Weis M, Kobinger GP, Becker S, von Messling V, Maisner A. 2016. Nipah virus matrix protein influences fusogenicity and is essential for particle infectivity and stability. J Virol 90:2514–2522. doi:10.1128/JVI.02920-15.

Editor: T. S. Dermody

Address correspondence to Andrea Maisner, maisner@staff.uni-marburg.de.

correct assembly of infectious cell-free NiV particles and influences the kinetics of cell-associated spread of NiV infection.

MATERIALS AND METHODS

Cells and viruses. Vero 76 cells (ATCC CRL1587) and 293 cells (ATCC CRL1573) were cultivated in Dulbecco's modified Eagle's medium (DMEM) with 10% fetal calf serum (FCS), 100 U of penicillin/ml, 0.1 mg of streptomycin/ml, and 4 mM glutamine (all from Life Technologies). All virus recovery and NiV infection experiments were performed in biosafety level 4 (BSL-4) containment at the Institute of Virology, Philipps University of Marburg, Marburg, Germany.

Generation of NiV full-length cDNA plasmids. Expression plasmids containing the nucleoprotein (N), phosphoprotein (P), and polymerase (L) protein were a kind gift of Markus Czub. To amplify fragments spanning the leader, trailer, and untranslated regions (UTRs), RNA isolated from Vero cells infected with NiV strain Malaysia (GenBank accession number NC_002728) was reverse transcribed using Superscript III (Invitrogen, Burlington, ON, Canada) using random hexamer primers. For the internal UTRs, the primers were chosen to include a unique or partially unique restriction site in each flanking gene. To introduce the eGFP in an additional transcription unit between G and L, the UTR between the P and M genes (PM UTR) was duplicated and inserted between the G and eGFP open reading frames, yielding pBRT7-NiVeG. The M gene-deleted derivative pBRT7-NiVeGΔM was produced by deleting the M open reading frame except for the stop codon to ensure that the rule of six was followed.

Recovery of recombinant viruses. To recover recombinant Nipah viruses, semiconfluent 293 cells in 6-well plates were infected with MVA-T7 at a multiplicity of infection (MOI) of 1. After 1 h at 37°C, medium was changed to 500 μl Opti-MEM. Then, cells were transfected with 0.75 μg pTM1-NiV N, 0.05 μg pTM1-NiV P, 0.4 μg pTM1-NiV L, and 5 μg pBR/T7-NiVeG or pBR/T7-NiVeGΔM, respectively, using Lipofectamine 2000 (Life Technologies). After 3 to 4 h at 37°C, medium was changed to DMEM–2% FCS with glutamine and antibiotics. If necessary, fresh 293 cells were added and medium was changed after 1 and 3 days, and the supernatant was transferred onto Vero cells after 6 to 9 days. Virus was harvested when 70 to 90% of the Vero cells showed cytopathic effects.

Virus titration, particle stability, and growth kinetics. Virus titers were quantified by limited dilution method and expressed as 50% tissue culture infections doses ($TCID_{50}$). To evaluate the particle stability, these titers were compared with titers obtained after 1 day or 5 days of incubation at 4°C or 37°C, respectively. For growth kinetics, confluent Vero cells seeded in 6-well plates were infected at an MOI of 0.001. After 1 h at 37°C, cells were washed 3 to 5 times, and samples from the supernatant were collected (t_0). Additional samples were collected and titrated after 24, 48, and 72 h. To compare cell-free and cell-associated virus titers, the cell culture supernatant was removed after 48 h, cleared for 10 min at 15,000 × *g* and used to determine cell-free virus titers. Infected cells were scraped into Opti-MEM and frozen at −80°C. After rapid thawing at 37°C, cell lysates were cleared by low-speed centrifugation, and cell-associated infectivity in the supernatants released by the freeze-thaw cycle was quantified. Viral titers ($n \geq 3$) were compared using an unpaired *t* test, performed in Microsoft Excel using the "T.TEST" function.

Live-cell imaging. To characterize the dissemination of the different viruses, Vero cells seeded in 35-mm μ-dishes (Ibidi, Munich) were infected with NiVeG or NiVeGΔM at an MOI of 0.005. After 1 h at 37°C, medium was replaced by CO_2-independent Leibovitz's medium without phenol red (Life Technologies) with 100 U/ml penicillin and 100 μg/ml streptomycin, 20% fetal bovine serum (FBS), and 400 μM 6-hydroxy-2,5,7,8-tetramethylchromane-2-carboxylic acid (Trolox; Sigma). Live-cell time-lapse experiments were started at 16 h after infection, and images were recorded with a Leica DMI6000B microscope using a 20× objective equipped with a remote control device to operate the microscope from outside the BSL-4 facility. Pictures were taken every 30 min and processed with Leica LAS AF software. The increase in size of a syncytium as a parameter for fusion kinetics was determined by measuring the area of 12 individual syncytia at different time points using ImageJ (http://rsbweb.nih.gov/ij). To calculate the relative increase, the area of the syncytium at 17 h after infection was set as 1.

MTT assay. The 3-(4,5-dimethyl-2-thiazolyl)-2,5-diphenyl-2H-tetrazolium bromide (MTT) assay was performed according to the manufacturer's protocol (Thermo Fisher Vybrant MTT Cell Proliferation Assay kit). Briefly, Vero cells grown in a 96-well plate were infected with NiVeG or NiVeGΔM at an MOI of 0.001 or 0.01. After 2 days, medium was replaced by phosphate-buffered saline (PBS) containing 1 mM MTT. After incubation for 4 h at 37°C, supernatants were removed, mixed with dimethyl sulfoxide (DMSO), and further incubated for 10 min at 37°C before absorption was measured at 562 nm using a PHOmo microplate reader. To calculate the relative cytotoxicity, the absorbance of uninfected cells was set to 1.

Quantification of NiV N RNA. Viral RNA was extracted from supernatants of NiVeG- or NiVeGΔM-infected Vero cells using the RNeasy kit (Qiagen) and reverse transcribed using Revert Aid H Minus Reverse Transcriptase (Fermentas). Real-time PCRs were performed in triplicates with a StepONE Plus cycler using QuantiFast SYBR green PCR master mix (Applied BioSystems) and NiV N-specific diagnostic primers. Genome numbers (2^{-Ct}; where *Ct* is the threshold cycle) and the infectivity-to-particle ratio, calculated by dividing the titer ($TCID_{50}$/ml) by 2^{-Ct}, were normalized to the values obtained for NiVeG (set as 1).

Virus purification and Western blot analysis. To evaluate viral protein expression levels, Vero cells were infected with NiVeG or NiVeGΔM at an MOI of 0.001. After 48 h, the supernatant was harvested and precleared by centrifugation for 10 min at 15,000 × *g*. Virus particles were then isolated by ultracentrifugation through a 20% sucrose cushion for 1.5 h at 150,000 × *g* and subsequent resuspension of the pellet in 30 μl 1% sodium dodecyl sulfate (SDS; Sigma) in PBS (Life Technologies). Cell lysates were collected at the same time by scraping the cells into 1% SDS in PBS. Two percent of the cell lysate and 33% of the virus pellet were then separated by reducing SDS-PAGE and transferred onto nitrocellulose. Membranes were incubated with polyclonal rabbit antisera directed against NiV G, F, and M peptides (G1126, F631, M1321; immunGlobe, Himmelstadt, Germany), followed by a biotin-labeled anti-rabbit antiserum and horseradish peroxidase (HRP)-conjugated streptavidin (Amersham). Bands were detected using a ChemiDoc (Bio-Rad). To stain NiV N, membranes were incubated with a polyclonal anti-NiV guinea pig serum (22). Primary antibodies were detected with an IRDye700-conjugated anti-guinea pig secondary antibody (LI-COR) and visualized with an Odyssey Imager (LI-COR).

PK protection assay. Two million Vero cells were infected with NiVeG or NiVeGΔM at an MOI of 0.001. After 48 h, supernatants were cleared for 10 min at 15,000 × *g* and subsequently centrifuged for 1 h at 150,000 × *g*. Virus pellets were resuspended in 60 μl PBS. Twenty microliters of the virus suspension either was left untreated (control) or was treated for 30 min at 37°C with proteinase K (PK) at a final concentration of 0.1 μg/μl in the absence or presence of 1% Triton X-100. Digestion was stopped by the addition of 1 μg/μl phenylmethylsulfonyl fluoride (PMSF). Samples were then inactivated and subjected to Western blot analysis using the polyclonal anti-NiV guinea pig serum.

Electron microscopy. For each virus, Vero cells grown to confluence in three 175-cm^2 flasks were infected with NiVeG or NiVeGΔM at an MOI of 0.005. After 48 h, virus particles were purified as outlined above, and the pellets were resuspended in 150 μl PBS. A drop of purified virus suspension was added on Formvar-coated nickel grids and incubated for 5 min. Then, samples were inactivated with 4% paraformaldehyde (PFA) for 2 days, and negative staining was performed with 2% phosphotungstic acid. Alternatively, grids were immunostained using a NiV-specific guinea pig serum and donkey anti-guinea pig secondary antibodies conjugated with 12-nm colloidal gold beads (Jackson ImmunoResearch, USA). Samples were analyzed by using a JEM 1400 transmission electron microscope at 120 kV.

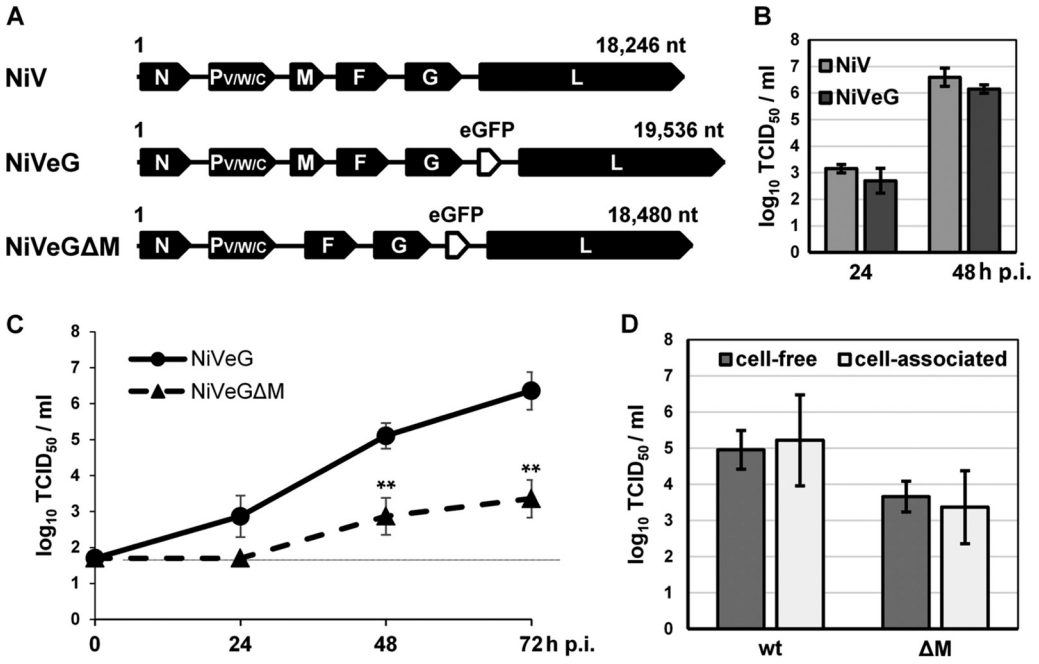

FIG 1 Characterization of recombinant eGFP-expressing wild-type and M protein-deleted NiV. (A) Schematic drawings of NiV, NiVeG, and NiVeGΔM full-length genomes in the cDNA plasmids. For all plasmids, the T7 RNA polymerase promoter is located immediately upstream of the genome, while the hepatitis δ ribozyme and T7 terminator are located immediately downstream of the genome to ensure correct genomic ends. nt, nucleotides. (B) Comparison of wild-type NiV and NiVeG titers. Vero cells were infected with recombinant wild-type NiV and NiVeG at a multiplicity of infection (MOI) of 0.001. Cell-free virus was quantified by the limited dilution method at 24 and 48 hpi, and titers are expressed as 50% tissue culture infectious doses ($TCID_{50}$/ml) ($n = 4$). Error bars indicate the standard deviations (SD). (C) Comparative growth kinetics of NiVeG and NiVeGΔM. Vero cells were infected at an MOI of 0.001. Cell-free virus titers were determined at 0, 24, 48, and 72 h ($n = 3$). The dotted line indicates the detection limit (50 $TCID_{50}$/ml). An unpaired *t* test was used to examine the significance of differences from NiVeG (**, $P < 0.01$). (D) Comparison of cell-free and cell-associated virus titers. Vero cells were infected with wild-type (wt) and M-deleted NiV (ΔM) at an MOI of 0.001. At 48 hpi, cell supernatants were harvested, cleared, and titrated (cell-free). Cells were scraped into Opti-MEM and subjected to one freeze-thaw cycle, and virus titers were quantified (cell-associated).

RESULTS

M gene-deleted NiV are released in the supernatant. While noninfectious systems have contributed importantly to the characterization of the henipavirus life cycle, several fundamental questions can be answered only by using recombinant viruses. So far, such genetically modified recombinant NiV have been used either to analyze the functions of V, W, or C proteins (23–25) or to characterize chimeric viruses in which NiV genes were exchanged by the homologous Hendra virus (HeV) genes (26). Here, we generated a replicative M gene-deleted NiV to characterize assembly and budding of infectious cell-free NiV particles in the total absence of M. Toward this, we generated a reverse genetics system based on the strategy used for the related morbilliviruses (27, 28). The entire genome of NiV Malaysia strain was assembled in a low-copy-number plasmid and flanked by a T7 promoter and a T7 terminator/hepatitis ∂ ribozyme cassette to ensure correct genome ends (Fig. 1A, NiV). An additional transcription unit carrying the eGFP gene was introduced between the G and L genes (NiVeG) to facilitate the detection of infected cells. To generate an M-deleted virus (NiVeGΔM), the M open reading frame was deleted from the NiVeG genomic plasmid (Fig. 1A).

All recombinant viruses could be recovered by transfecting the respective genomic plasmid with T7 polymerase-driven expression plasmids for the N, P, and L proteins in 293 cells previously infected with MVA-T7, which provided the T7 polymerase. Interestingly, NiVeGΔM could be rescued and propagated without transcomplementation of plasmid-encoded M protein. While the replication efficacies of recombinant NiV and NiVeG were similar, indicating that introduction of the GFP cassette did not affect virus growth (Fig. 1B), NiVeGΔM was associated with 10- to 1,000-fold-lower titers (Fig. 1C). Since the maximal cell-associated infectivity was similarly reduced (Fig. 1D), this cannot be explained by just a budding defect in the absence of M. Instead, it indicates that the M protein is required for proper assembly of infectious particles.

Absence of M protein results in enhanced syncytium formation kinetics. While deletion of Sendai virus or measles virus (MV) M genes caused an increased fusogenicity and resulted in the formation of much larger syncytia (20, 29), no influence on the cytopathic effect was observed for a human respiratory syncytial virus (HRSV) lacking the M protein (21). Phase-contrast microscopy suggested a slightly enhanced fusogenicity of NiVeGΔM. However, because of the heterogeneous sizes of syncytia at any steady-state time point after infection, the differences in average syncytium sizes were not statistically significant (data not shown). We therefore performed a live-cell imaging analysis of Vero cells infected with NiVeG and NiVeGΔM. By monitoring individual syncytia over 2 days, we analyzed fusion kinetics to determine the influence of M deletion on the progression of NiV-mediated cell-cell fusion. For both viruses, the first syncytia encompassing 2 to 5 cells were detected 17 h after infection (Fig. 2A). There was a gradual increase in syncytium sizes over time for both viruses, but

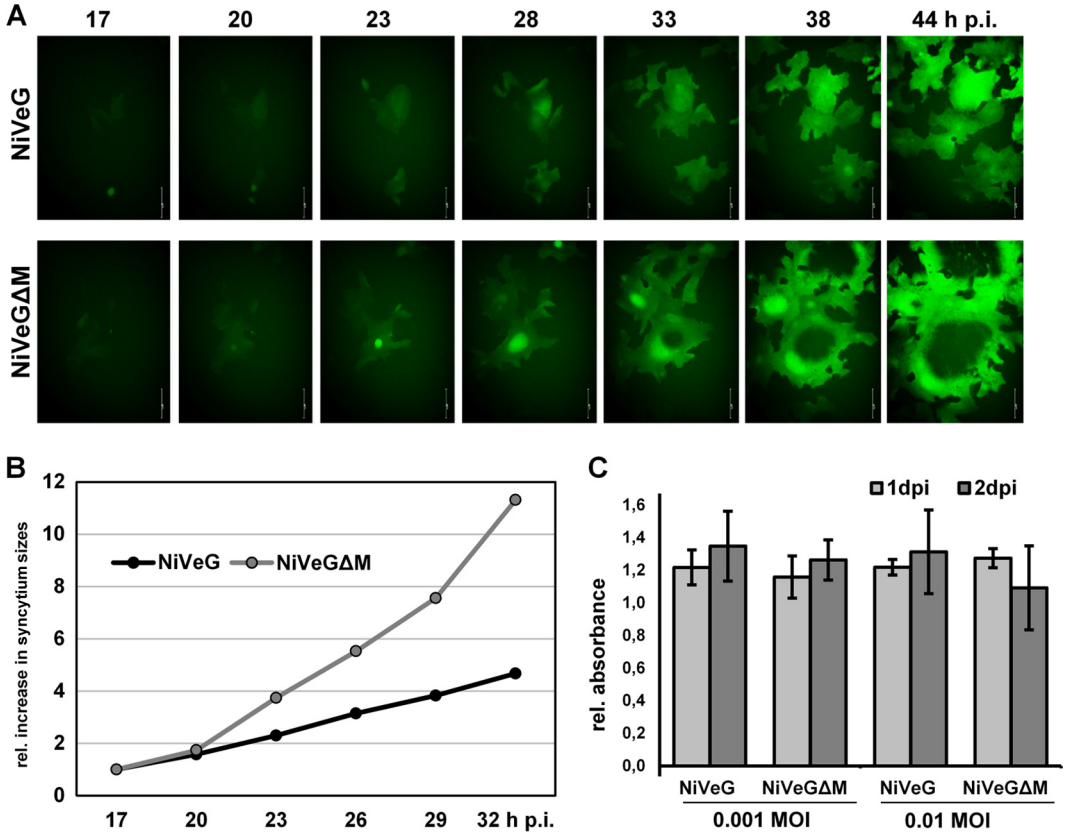

FIG 2 Live-cell microscopy to monitor NiVeG and NiVeGΔM cell-to-cell fusion kinetics. Vero cells were infected with NiVeG and NiVeGΔM at an MOI of 0.005. Time-lapse microscopy was started 16 h later, and GFP fluorescence signals were recorded every 30 min with a Leica DMI6000B microscope. (A) Selected images of the same microscopic field are shown for the indicated time points. Magnification, ×200. Bar, 100 μm. (B) Quantitative fusion kinetics. Areas of single syncytia were measured at different time points after infection ($n = 12$). To calculate the relative increase in size, the area of the syncytium after 17 h was set to 1. Significance of difference between NiVeG and NiVeGΔM, $P < 0.1$. (C) Effect of NiVeG and NiVeGΔM infection on cell viability. MTT assays were performed with Vero cells infected at an MOI of 0.001 or 0.01 at 24 h and 48 h after infection. Data were normalized to uninfected cells. Means and SD are shown. Student's *t* test analysis did not reveal any statistically significant differences.

fusion kinetics was more pronounced for NiVeGΔM (Fig. 2B). Though syncytia generally grew faster due to the increased fusogenicity of NiVeGΔM, this did not result in an enhanced cytotoxic effect. Cell viability of NiVeG- and NiVeGΔM-infected cells at 24 h and 48 h postinfection (hpi) did not differ significantly (Fig. 2C). As in Vero cells, we observed an enhanced fusogenicity of NiVeGΔM in A549 cells (data not shown). Together, these results illustrate that the NiV M protein modulates glycoprotein-mediated cell-to-cell fusion to a greater extent than the M protein of HRSV, albeit to a lesser extent than the M proteins of Sendai virus or MV.

M protein deletion causes the formation of less-infectious particles with reduced stability. To determine if reduced NiVeGΔM titers are the result of less efficient particle formation or of a difference in particle infectivity, we compared the amounts of viral RNA in the supernatants of NiVeG- and of NiVeGΔM-infected cells, in which infectious titers of the latter were about 100-fold reduced. Real-time reverse transcription (RT)-PCR analysis (qPCR) with NiV N-specific primers revealed an increased relative particle/genome number in the supernatant of NiVeGΔM-infected cells (Fig. 3A, left panel). Setting the infectivity-to-particle ratio of NiVeG to 1, NiVeGΔM thus yielded a relative infectivity between 0.001 and 0.01 (Fig. 3A, right panel). To evaluate if differences in viral protein expression account for this observation, we analyzed the NiV protein expression in infected cell lysates and the particle composition. As expected, the M protein was absent in NiVeGΔM-infected cells and the resulting viral particles (Fig. 3B, lanes 3 and 4). While the viral protein content in infected cells was otherwise not affected by the absence of M (Fig. 3B, lanes 1 and 3), the total amount of G, F, and N proteins in the purified viral particle fraction was considerably higher for NiVeGΔM (Fig. 3B, lanes 4 and 2). As shown in the Coomassie blue-stained gel (Fig. 3C), NiVeGΔM virus preparations contained not only larger amounts of viral proteins but also a substantially increased amount of total (cellular) proteins (Fig. 3C). Proteinase K (PK) digestion in the absence and presence of TX-100 confirmed that particles with incorporated N protein are present in NiVeG and NiVeGΔM supernatants (Fig. 3D). However, compared to PK-treated NiVeG particles, the relative amount of N protein in PK-digested NiVeGΔM particles was reduced. This might hint on a compromised viral membrane integrity when M is absent.

To assess if M depletion affects not only the composition of cell-free virus preparations but also their thermostability, we compared the infectivity of NiVeG and NiVeGΔM after incubation at 4°C with that at 37°C. While the infectious titers of both viruses

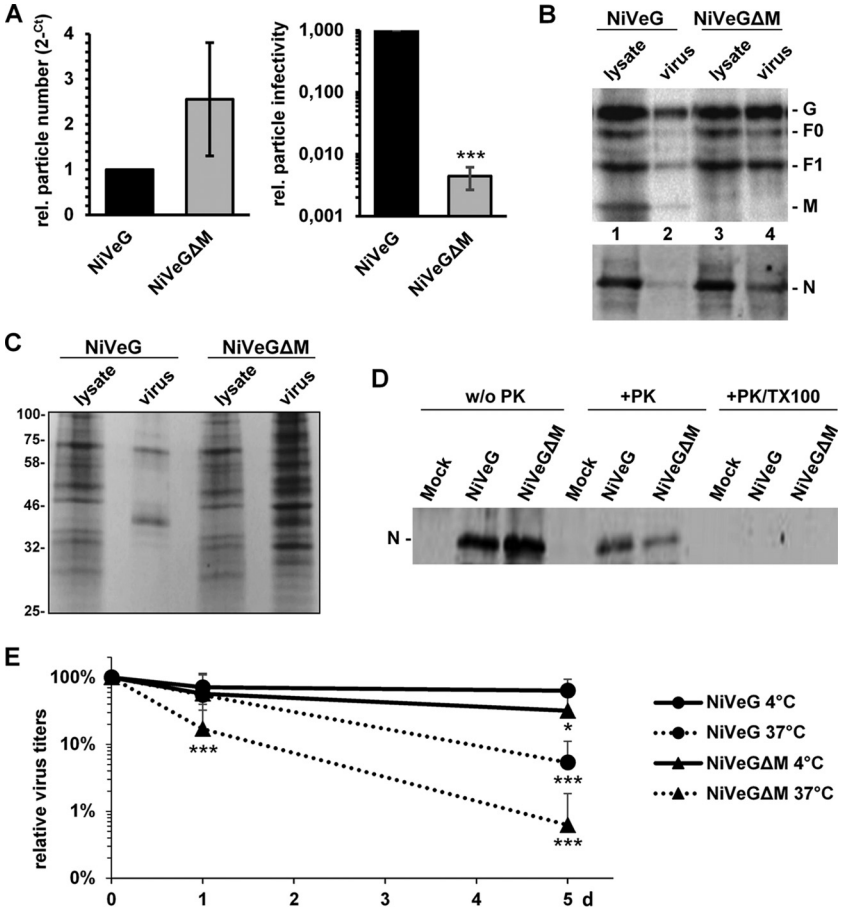

FIG 3 Comparison of particle infectivity, protein composition, protease resistance, and thermostability. (A) Relative particle numbers and infectivity-to-particle ratios of NiVeG and NiVeGΔM. Cell-free virus titers were quantified, and RNA was isolated from 100 μl supernatant of infected cells after 48 h. Genomic RNA was quantified by qRT-PCR using NiV N-specific primers. The relative particle/genome numbers (2^{-Ct}) normalized to NiVeG (set as 1) are shown in the left panel. The infectivity-to-particle ratio was calculated by dividing the titer ($TCID_{50}$/ml) by genome numbers (2^{-Ct}) and was normalized to the values obtained for NiVeG (set as 1) to get the relative particle infectivity (right panel). Error bars indicate the standard deviations ($n = 3$). Statistical significance is indicated by asterisks (***, $P < 0.001$). (B, C) Viral protein content in infected cells and purified particles. Infected Vero cells were lysed at 48 h after infection, and cell-free virus was purified from cell supernatants. For each virus, 2% of the total cell lysates and 33% of the purified particles were separated on 10% SDS-PAGE gels. (B) To specifically detect viral proteins, one gel was blotted to nitrocellulose. Viral proteins were detected by Western blotting using NiV M-, F-, and G-specific antisera and HRP-conjugated secondary antibodies. Chemiluminescent signals were recorded with a Chemidoc system (upper panel). NiV N protein was visualized with a polyclonal NiV-specific guinea pig serum and IRDye700-labeled secondary antibodies. Signals were recorded with an Odyssey Imaging system (bottom panel). (C) To visualize all proteins in cell lysates and virus pellets, one gel was stained with Coomassie blue. (D) Proteinase K protection assay. At 48 h after infection, virus particles were pelleted from clarified cell supernatants, suspended in PBS, and either left untreated (w/o PK) or treated with proteinase K in the absence (+PK) or presence (+PK/TX100) of Triton X-100. The samples were then analyzed by Western blotting using polyclonal NiV-specific antibodies as described above. (E) Stability of NiVeG and NiVeGΔM infectivity at different temperatures. Cell-free virus was incubated for the indicated times at 4°C or 37°C, respectively. Titers at day (d) 0 were set as 100% and used for the calculation of the relative loss in virus titers. Error bars indicate the standard deviations ($n = 3$). Statistical significance is indicated by asterisks (*, $P < 0.05$; ***, $P < 0.001$).

remained almost stable for 5 days at 4°C, incubation for 24 h at 37°C had little effect on the parental NiVeG but resulted in a statistically highly significant 10-fold drop in titers for NiVeGΔM (Fig. 3E). After 5 days at 37°C, infectivity of NiVeGΔM was reduced more than 100-fold, while NiVeG titers had dropped only 10-fold (Fig. 3E). Taken together, this supports the idea that in the absence of M, the coordinated assembly of largely cell protein-free virus virions is disturbed, resulting in the production of cell-free NiVeGΔM particles with increased cellular protein incorporation and lower particle stability.

The M protein coordinates the budding process. To gain more-detailed insights in the morphology of the released particles, we performed a negative-stain transmission electron microscopy (EM) analysis of cell-free virus preparations from NiVeG- and NiVeGΔM-infected cell supernatants at 48 h after infection. Consistent with the detection of increased viral and cellular protein amounts by Western blotting and Coomassie blue staining (Fig. 3B and C), virus preparations pelleted from supernatants of NiVeGΔM-infected cells contained a dramatically increased amount of vesicular material compared to that in NiVeG virus preparations (Fig. 4A and B). For a more in-depth characterization of the particle morphology, we analyzed NiVeG and NiVeGΔM samples by immuno-EM using a polyclonal anti-NiV guinea pig antiserum. In both virus preparations, we found particles heavily decorated with immunogold beads. Among them were spherical, filamentous, and pleomorphic virions, as previ-

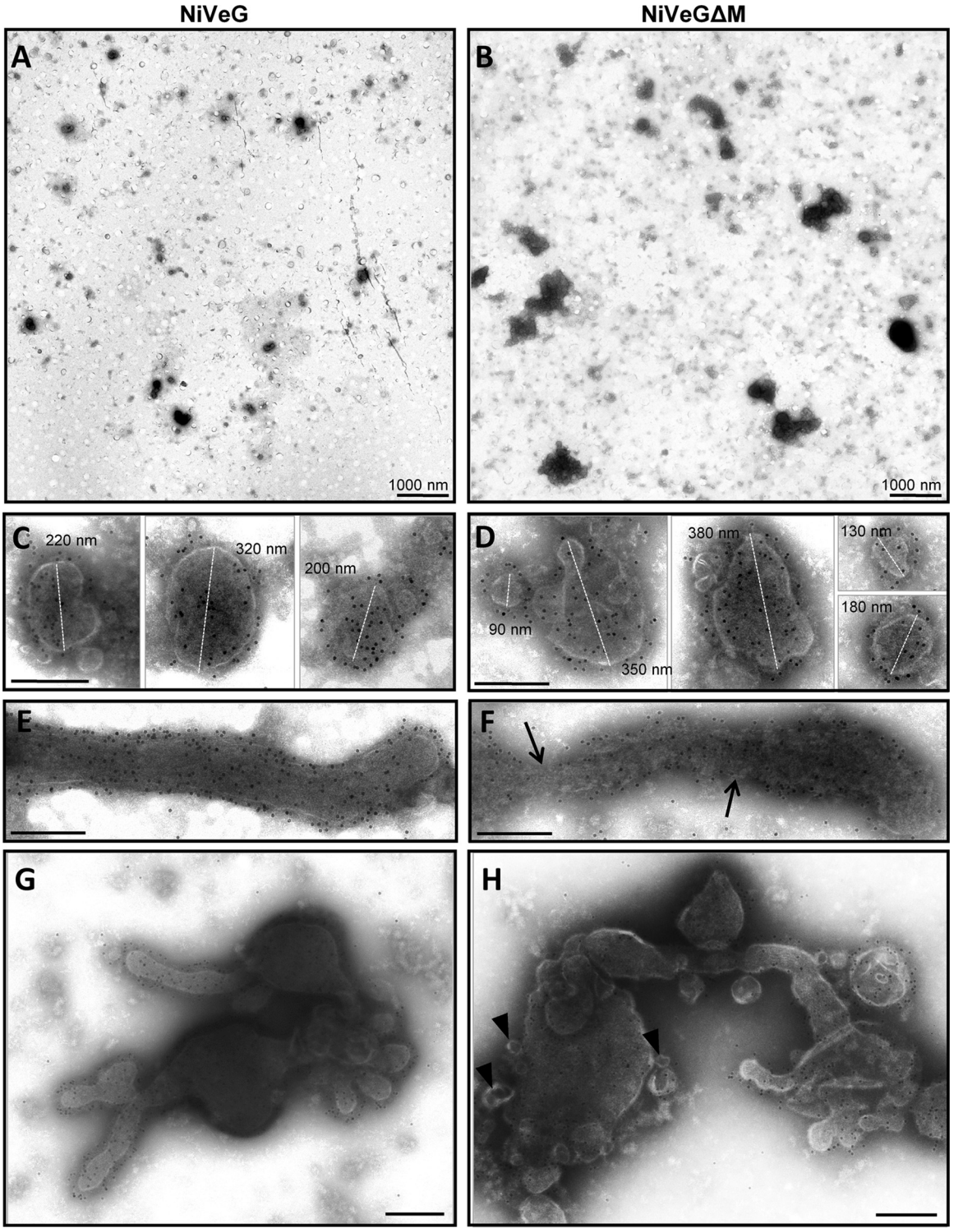

FIG 4 Ultrastructural analysis of viruses from cell supernatants. Vero cells were infected with NiVeG and NiVeGΔM at an MOI of 0.005 for 48 h. Virus particles were purified from the supernatant by centrifugation over a 20% sucrose cushion, fixed, and inactivated for 48 h in 4% paraformaldehyde. (A, B) Samples were subjected to negative staining with 2% phosphotungstic acid. Bars, 1 μm. (C to H) Virus preparations were analyzed by immunoelectron microscopy using a NiV-specific polyclonal guinea pig antiserum and secondary antibodies coupled with 12-nm colloidal gold beads, followed by negative staining. (C, D) Spherical viral particles. Dashed lines indicate the positions of the measured diameters. (E, F) Filamentous viral particles. Arrows show defects in the integrity of virus envelope. (G, H) Pleomorphic particles. Arrowheads indicate membrane blebs. Bars, 200 nm.

ously described by Hyatt et al. (30). Spherical NiVeG and NiVeGΔM particle sizes both ranged from 90 to 380 nm (Fig. 4C and D), and filamentous NiVeG and NiVeGΔM particles also had similar total sizes (Fig. 4E and F). However, these elongated NiVeGΔM particles had a more irregular shape and displayed some defects in the particle envelope (Fig. 4F, arrows), which supports the idea of a compromised membrane integrity suggested by the PK digestion (Fig. 3D). Similar to filamentous particles, NiVeGΔM particles with pleomorphic shapes differed from pleomorphic NiVeG by a more irregular morphology, an uneven surface, and some envelope blebs (Fig. 4G and H), indicating a less coordinated budding process in the absence of M.

DISCUSSION

The characterization of NiV assembly in the total absence of the M protein has thus far relied on the coexpression of recombinant proteins outside the authentic viral context. To address this limitation, we established a reverse genetics system based on NiV strain Malaysia. Using the system, we were able to recover NiVeGΔM, an eGFP-expressing derivative lacking the M protein transcription unit. While the fusogenicity of NiVeGΔM was slightly enhanced, replication kinetics was significantly impaired. Together with the release of large amounts of viral and cellular proteins and the severely reduced infectivity and stability, our data indicate that the M protein is essential for proper NiV particle assembly, consistent with its role in other paramyxoviruses (21, 31–33).

Requirements for VLP and infectious particle formation are different. Virus-like particles are frequently used to investigate the assembly mechanisms of enveloped viruses (34). For NiV, expression of the F or G protein alone is sufficient to yield VLPs in the supernatant, and the coexpression of M greatly increases the efficiency of VLP formation (13, 35). This intrinsic budding activity of the F and G proteins is likely the origin of the large amount of viral protein detected in purified supernatant of NiVeGΔM-infected cells. However, the low infectivity-to-particle ratio indicates that these M protein-independent budding activities only accidentally generate infectious RNP-containing particles while mostly yielding noninfectious virus-like particles also found in F/G expression systems. Furthermore, it is likely that the envelope of the few RNP-containing particles produced in the absence of the M protein has a suboptimal composition of surface glycoproteins, which may impair the virus entry and uncoating processes (11, 21). Whether the role of the M protein in the assembly process is mainly to concentrate viral components at specific sites at the plasma membrane or to ensure a defined stoichiometry of RNPs, G and F proteins require further investigation.

Conserved and divergent functions of paramyxovirus M proteins. Despite their conserved role in assembly and budding, there are genus- and strain-specific differences between paramyxoviral matrix proteins that do not allow exchanging M proteins even between closely related viruses without affecting virus growth (36–38). In line with these studies, a recent cross-complementation study by Yun et al. (26) demonstrated that introduction of the Hendra virus M gene into NiV increased the replicative titers, likely as a result of an increased budding activity of HeV M.

While some attempts to generate members of the *Paramyxoviridae* family without complementation of functional M proteins were not successful (31–33), M protein-deleted measles (MVΔM) and respiratory syncytial (M-null HRSV) viruses have been recovered (20, 21). While M-null HRSV was completely defective in virus budding (21), limited amounts of infectious MVΔM were found in the supernatant (20), indicating a varying importance of the M protein contribution among different genera.

In line with what has been reported for MVΔM (20), we observed an increased fusogenicity for NiVeGΔM. Although the effect of M depletion on NiV-mediated cell-cell fusion is clearly less pronounced, it may be speculated that as in MV infection (39, 40), NiV M downregulates cell-cell fusion by interacting with the cytoplasmic portions of the NiV surface glycoproteins. In contrast to the increased fusogenicity seen in M-deficient MV, Sendai virus, and NiV, deletion of the HRSV M protein did not result in enhanced fusion (21), suggesting that paramyxovirus M proteins differentially influence cell-to-cell fusion. In polarized cell types, the role of M proteins might be even more diverse. Due to the polarized nature of epithelial and endothelial target tissues, viral proteins and RNPs are often specifically transported to apical or basolateral membrane domains. In the case of NiV, NiV F and G proteins contain cytoplasmic sorting signals that lead to a basolateral targeting upon single expression. In the viral context, however, both glycoproteins are expressed in a more apical fashion. This redistribution is assumed to be caused by the NiV M that is selectively targeted to the apical surface of polarized cells (14, 41, 42). This M-driven apical accumulation of all viral components is thought to ensure efficient apical NiV budding while downregulating F/G-dependent lateral cell-to-cell fusion kinetics within the polarized cell monolayer. Future studies will determine the effect of M deficiency on unipolar NiV budding and fusion downregulation in polarized endothelial and epithelial cell types.

ACKNOWLEDGMENTS

All work with live NiV was performed in the BSL-4 facility of Philipps University, Marburg, Germany. We thank Markus Czub and Heinz Feldmann for providing NiV plasmids and guinea pig antisera. We also thank all laboratory members, especially Marc Ringel and Boris Lamp, for continuing support and lively discussions.

FUNDING INFORMATION

Deutsche Forschungsgemeinschaft (DFG) provided funding to Andrea Maisner under grant numbers MA 1886/6-2 and SFB 1021 TP B04. Gouvernement du Canada | Canadian Institutes of Health Research (CIHR) provided funding to Veronika von Messling under grant number MOP66989. Bundesministerium für Gesundheit (BMG) provided funding to Veronika von Messling.

The funders had no role in study design, data collection and interpretation, or the decision to submit the work for publication.

REFERENCES

1. **Chua KB, Goh KJ, Wong KT, Kamarulzaman A, Tan PS, Ksiazek TG, Zaki SR, Paul G, Lam SK, Tan CT.** 1999. Fatal encephalitis due to Nipah virus among pig-farmers in Malaysia. Lancet **354:**1257–1259. http://dx.doi.org/10.1016/S0140-6736(99)04299-3.
2. **Luby SP, Hossain MJ, Gurley ES, Ahmed BN, Banu S, Khan SU, Homaira N, Rota PA, Rollin PE, Comer JA, Kenah E, Ksiazek TG, Rahman M.** 2009. Recurrent zoonotic transmission of Nipah virus into humans, Bangladesh, 2001-2007. Emerg Infect Dis **15:**1229–1235. http://dx.doi.org/10.3201/eid1508.081237.
3. **Baker KS, Todd S, Marsh GA, Crameri G, Barr J, Kamins AO, Peel AJ, Yu M, Hayman DT, Nadjm B, Mtove G, Amos B, Reyburn H, Nyarko E, Suu-Ire R, Murcia PR, Cunningham AA, Wood JL, Wang LF.** 2013. Novel, potentially zoonotic paramyxoviruses from the African straw-

colored fruit bat Eidolon helvum. J Virol **87:**1348–1358. http://dx.doi.org/10.1128/JVI.01202-12.

4. **Drexler JF, Corman VM, Gloza-Rausch F, Seebens A, Annan A, Ipsen A, Kruppa T, Müller MA, Kalko EK, Adu-Sarkodie Y, Oppong S, Drosten C.** 2009. Henipavirus RNA in African bats. PLoS One **4:**e6367. http://dx.doi.org/10.1371/journal.pone.0006367.
5. **Hasebe F, Thuy NT, Inoue S, Yu F, Kaku Y, Watanabe S, Akashi H, Dat DT, Mai lT, Morita K.** 2012. Serologic evidence of nipah virus infection in bats, Vietnam. Emerg Infect Dis **18:**536–537. http://dx.doi.org/10.3201/eid1803.111121.
6. **Hayman DT, Suu-Ire R, Breed AC, McEachern JA, Wang L, Wood JL, Cunningham AA.** 2008. Evidence of henipavirus infection in West African fruit bats. PLoS One **3:**e2739. http://dx.doi.org/10.1371/journal.pone.0002739.
7. **Hayman DT, Wang LF, Barr J, Baker KS, Suu-Ire R, Broder CC, Cunningham AA, Wood JL.** 2011. Antibodies to henipavirus or henipa-like viruses in domestic pigs in Ghana, West Africa. PLoS One **6:**e25256. http://dx.doi.org/10.1371/journal.pone.0025256.
8. **Iehle C, Razafitrimo G, Razainirina J, Andriaholinirina N, Goodman SM, Faure C, Georges-Courbot MC, Rousset D, Reynes JM.** 2007. Henipavirus and Tioman virus antibodies in pteropodid bats, Madagascar. Emerg Infect Dis **13:**159–161. http://dx.doi.org/10.3201/eid1301.060791.
9. **Peel AJ, Baker KS, Crameri G, Barr JA, Hayman DT, Wright E, Broder CC, Fernández-Loras A, Fooks AR, Wang LF, Cunningham AA, Wood JL.** 2012. Henipavirus neutralising antibodies in an isolated island population of African fruit bats. PLoS One **7:**e30346. http://dx.doi.org/10.1371/journal.pone.0030346.
10. **Reynes JM, Counor D, Ong S, Faure C, Seng V, Molia S, Walston J, Georges-Courbot MC, Deubel V, Sarthou JL.** 2005. Nipah virus in Lyle's flying foxes, Cambodia. Emerg Infect Dis **11:**1042–1047. http://dx.doi.org/10.3201/eid1107.041350.
11. **El Najjar F, Schmitt AP, Dutch RE.** 2014. Paramyxovirus glycoprotein incorporation, assembly and budding: a three way dance for infectious particle production. Viruses **6:**3019–3054. http://dx.doi.org/10.3390/v6083019.
12. **Ciancanelli MJ, Basler CF.** 2006. Mutation of YMYL in the Nipah virus matrix protein abrogates budding and alters subcellular localization. J Virol **80:**12070–12078. http://dx.doi.org/10.1128/JVI.01743-06.
13. **Patch JR, Crameri G, Wang LF, Eaton BT, Broder CC.** 2007. Quantitative analysis of Nipah virus proteins released as virus-like particles reveals central role for the matrix protein. Virol J **4:**1. http://dx.doi.org/10.1186/1743-422X-4-1.
14. **Lamp B, Dietzel E, Kolesnikova L, Sauerhering L, Erbar S, Weingartl H, Maisner A.** 2013. Nipah virus entry and egress from polarized epithelial cells. J Virol **87:**3143–3154. http://dx.doi.org/10.1128/JVI.02696-12.
15. **Bauer A, Neumann S, Karger A, Henning AK, Maisner A, Lamp B, Dietzel E, Kwasnitschka L, Balkema-Buschmann A, Keil GM, Finke S.** 2014. ANP32B is a nuclear target of henipavirus M proteins. PLoS One **9:**e97233. http://dx.doi.org/10.1371/journal.pone.0097233.
16. **Pentecost M, Vashisht AA, Lester T, Voros T, Beaty SM, Park A, Wang YE, Yun TE, Freiberg AN, Wohlschlegel JA, Lee B.** 2015. Evidence for ubiquitin-regulated nuclear and subnuclear trafficking among Paramyxovirinae matrix proteins. PLoS Pathog **11:**e1004739. http://dx.doi.org/10.1371/journal.ppat.1004739.
17. **Wang YE, Park A, Lake M, Pentecost M, Torres B, Yun TE, Wolf MC, Holbrook MR, Freiberg AN, Lee B.** 2010. Ubiquitin-regulated nuclear-cytoplasmic trafficking of the Nipah virus matrix protein is important for viral budding. PLoS Pathog **6:**e1001186. http://dx.doi.org/10.1371/journal.ppat.1001186.
18. **Sun W, McCrory TS, Khaw WY, Petzing S, Myers T, Schmitt AP.** 2014. Matrix proteins of Nipah and Hendra viruses interact with beta subunits of AP-3 complexes. J Virol **88:**13099–13110. http://dx.doi.org/10.1128/JVI.02103-14.
19. **Patch JR, Han Z, McCarthy SE, Yan L, Wang LF, Harty RN, Broder CC.** 2008. The YPLGVG sequence of the Nipah virus matrix protein is required for budding. Virol J **5:**137. http://dx.doi.org/10.1186/1743-422X-5-137.
20. **Cathomen T, Mrkic B, Spehner D, Drillien R, Naef R, Pavlovic J, Aguzzi A, Billeter MA, Cattaneo R.** 1998. A matrix-less measles virus is infectious and elicits extensive cell fusion: consequences for propagation in the brain. EMBO J **17:**3899–3908. http://dx.doi.org/10.1093/emboj/17.14.3899.
21. **Mitra R, Baviskar P, Duncan-Decocq RR, Patel D, Oomens AG.** 2012. The human respiratory syncytial virus matrix protein is required for maturation of viral filaments. J Virol **86:**4432–4443. http://dx.doi.org/10.1128/JVI.06744-11.
22. **Thiel L, Diederich S, Erbar S, Pfaff D, Augustin HG, Maisner A.** 2008. Ephrin-B2 expression critically influences Nipah virus infection independent of its cytoplasmic tail. Virol J **5:**163. http://dx.doi.org/10.1186/1743-422X-5-163.
23. **Yoneda M, Guillaume V, Sato H, Fujita K, Georges-Courbot MC, Ikeda F, Omi M, Muto-Terao Y, Wild TF, Kai C.** 2010. The nonstructural proteins of Nipah virus play a key role in pathogenicity in experimentally infected animals. PLoS One **5:**e12709. http://dx.doi.org/10.1371/journal.pone.0012709.
24. **Mathieu C, Guillaume V, Volchkova VA, Pohl C, Jacquot F, Looi RY, Wong KT, Legras-Lachuer C, Volchkov VE, Lachuer J, Horvat B.** 2012. Nonstructural Nipah virus C protein regulates both the early host proinflammatory response and viral virulence. J Virol **86:**10766–10775. http://dx.doi.org/10.1128/JVI.01203-12.
25. **Ciancanelli MJ, Volchkova VA, Shaw ML, Volchkov VE, Basler CF.** 2009. Nipah virus sequesters inactive STAT1 in the nucleus via a P gene-encoded mechanism. J Virol **83:**7828–7841. http://dx.doi.org/10.1128/JVI.02610-08.
26. **Yun T, Park A, Hill TE, Pernet O, Beaty SM, Juelich TL, Smith JK, Zhang L, Wang YE, Vigant F, Gao J, Wu P, Lee B, Freiberg AN.** 2015. Efficient reverse genetics reveals genetic determinants of budding and fusogenic differences between Nipah and Hendra viruses and enables real-time monitoring of viral spread in small animal models of Henipavirus infection. J Virol **89:**1242–1253. http://dx.doi.org/10.1128/JVI.02583-14.
27. **Radecke F, Spielhofer P, Schneider H, Kaelin K, Huber M, Dotsch C, Christiansen G, Billeter MA.** 1995. Rescue of measles viruses from cloned DNA. EMBO J **14:**5773–5784.
28. **von Messling V, Zimmer G, Herrler G, Haas L, Cattaneo R.** 2001. The hemagglutinin of canine distemper virus determines tropism and cytopathogenicity. J Virol **75:**6418–6427. http://dx.doi.org/10.1128/JVI.75.14.6418-6427.2001.
29. **Inoue M, Tokusumi Y, Ban H, Kanaya T, Shirakura M, Tokusumi T, Hirata T, Nagai Y, Iida A, Hasegawa M.** 2003. A new Sendai virus vector deficient in the matrix gene does not form virus particles and shows extensive cell-to-cell spreading. J Virol **77:**6419–6429. http://dx.doi.org/10.1128/JVI.77.11.6419-6429.2003.
30. **Hyatt AD, Zaki SR, Goldsmith CS, Wise TG, Hengstberger SG.** 2001. Ultrastructure of Hendra virus and Nipah virus within cultured cells and host animals. Microbes Infect **3:**297–306. http://dx.doi.org/10.1016/S1286-4579(01)01383-1.
31. **Mottet G, Mühlemann A, Tapparel C, Hoffmann F, Roux L.** 1996. A Sendai virus vector leading to the efficient expression of mutant M proteins interfering with virus particle budding. Virology **221:**159–171. http://dx.doi.org/10.1006/viro.1996.0362.
32. **Mottet-Osman G, Iseni F, Pelet T, Wiznerowicz M, Garcin D, Roux L.** 2007. Suppression of the Sendai virus M protein through a novel short interfering RNA approach inhibits viral particle production but does not affect viral RNA synthesis. J Virol **81:**2861–2868. http://dx.doi.org/10.1128/JVI.02291-06.
33. **Zhang G, Zhang S, Ding B, Yang X, Chen L, Yan Q, Jiang Y, Zhong Y, Chen M.** 2014. A leucine residue in the C terminus of human parainfluenza virus type 3 matrix protein is essential for efficient virus-like particle and virion release. J Virol **88:**13173–13188. http://dx.doi.org/10.1128/JVI.01485-14.
34. **Harrison MS, Sakaguchi T, Schmitt AP.** 2010. Paramyxovirus assembly and budding: building particles that transmit infections. Int J Biochem Cell Biol **42:**1416–1429. http://dx.doi.org/10.1016/j.biocel.2010.04.005.
35. **Landowski M, Dabundo J, Liu Q, Nicola AV, Aguilar HC.** 2014. Nipah virion entry kinetics, composition, and conformational changes determined by enzymatic virus-like particles and new flow virometry tools. J Virol **88:**14197–14206. http://dx.doi.org/10.1128/JVI.01632-14.
36. **Dietzel E, Anderson DE, Castan A, von Messling V, Maisner A.** 2011. Canine distemper virus matrix protein influences particle infectivity, particle composition, and envelope distribution in polarized epithelial cells and modulates virulence. J Virol **85:**7162–7168. http://dx.doi.org/10.1128/JVI.00051-11.
37. **Mahapatra M, Parida S, Baron MD, Barrett T.** 2006. Matrix protein and glycoproteins F and H of Peste-des-petits-ruminants virus function better as a homologous complex. J Gen Virol **87:**2021–2029. http://dx.doi.org/10.1099/vir.0.81721-0.
38. **Sharma LB, Ohgimoto S, Kato S, Kurazono S, Ayata M, Takeuchi K,**

Ihara T, Ogura H. 2009. Contribution of matrix, fusion, hemagglutinin, and large protein genes of the CAM-70 measles virus vaccine strain to efficient growth in chicken embryonic fibroblasts. J Virol **83:**11645–11654. http://dx.doi.org/10.1128/JVI.01110-09.

39. **Cathomen T, Naim HY, Cattaneo R.** 1998. Measles viruses with altered envelope protein cytoplasmic tails gain cell fusion competence. J Virol **72:**1224–1234.
40. **Moll M, Klenk HD, Maisner A.** 2002. Importance of the cytoplasmic tails of the measles virus glycoproteins for fusogenic activity and the generation of recombinant measles viruses. J Virol **76:**7174–7186. http://dx.doi.org/10.1128/JVI.76.14.7174-7186.2002.
41. **Erbar S, Maisner A.** 2010. Nipah virus infection and glycoprotein targeting in endothelial cells. Virol J **7:**305. http://dx.doi.org/10.1186/1743-422X-7-305.
42. **Weise C, Erbar S, Lamp B, Vogt C, Diederich S, Maisner A.** 2010. Tyrosine residues in the cytoplasmic domains affect sorting and fusion activity of the Nipah virus glycoproteins in polarized epithelial cells. J Virol **84:**7634–7641. http://dx.doi.org/10.1128/JVI.02576-09.